Chapter-6

Electrochemical behaviour of Sn-9Zn-xCu solder alloy in 3.5wt. % NaCl solution at room temperature

6.1 Introduction

Sn–9Zn alloy has been seen as one an essential alternate lead-free solder alloy because of its low melting temperature (198.5°C), extremely near to that of Sn–37Pb alloy (183°C); it also exhibits good mechanical properties and low cost [163][164]. On the other hand, Sn–Zn alloys have various drawbacks that limit their application and keep them from finding broad use in electronic assemblies.

Generally, soldiers are exposed to corrosive environments such as air, ocean, moisture, and air pollutants. This raises concerns about the durability of the joints due to corrosion. Therefore excellent corrosion resistance is necessary for solder materials to provide high connection dependability. On the other hand, Sn-Zn solders have chemically active Zn, which readily reacts with gas and moisture in the air, resulting in a high corrosion rate. Until now, the majority of Sn-Zn alloy research has concentrated on mechanical properties and Physico-chemical performance [165][166][167][168], with relatively little investigation into corrosion performance [83]. According to prior research, the coarse Zn phase in the Sn matrix increases pitting susceptibility and decreases corrosion resistance. Therefore, removing the coarse Zn phase is expected to improve corrosion performance while maintaining or even improving the Sn-Zn solder's other properties [72]. As a result, if Sn–Zn-based solder alloys are to be widely used in electronic components, they must improve their corrosion resistance. The literature found that the addition of alloying elements can be a successful method for modifying various properties of solder alloys [81][2]. For example, additions of In and Bi are intended to reduce the melting point while improving the wetting properties of Sn–Zn solder alloys [169][170]. However, it was reported in the literature that adding Bi resulted in decreased oxidation resistance and joint degeneration when exposed to heat and humidity [171]. The Only way to have suitable Sn–Zn solders is to form Zn-containing intermetallics to prevent the formation of

coarse Zn-rich precipitates intermetallic compound (IMC). According to Yu et al.[172], the wetting behaviour of the Sn–9Zn–xCu has improved significantly as the Cu concentration increased, which was attributable to reduced liquid surface tension resulting from the development of Cu–Zn (IMC) [173][174].

As a result, the current research investigates the feasibility of creating Sn-9Zn-xCu solder alloys and electrochemical behaviour in sodium chloride solution. Although Liu. et al. [75] indicated that only 1 wt.% Cu addition had a significant impact on the corrosion properties of Sn-9Zn solder alloy. A few investigations on the influence of copper on the corrosion parameters of Sn-Zn solder alloys were reported in the literature. To analyze the influence of copper on the corrosion performance of the Sn-9Zn-xCu (x=0, 1, 2 & 3 wt. %) alloys were synthesized, and the electrochemical behaviour in 3.5 wt.% simulated NaCl at ambient temperature was investigated using potentiodynamic polarization and EIS techniques. X-ray diffraction (XRD) and scanning electron microscopy (SEM) equipped with an Energy Dispersive X-ray (EDX) and X-ray photoelectron spectroscopy (XPS) were used to learn more about the surface composition, morphology, and chemical state of various products generated by corrosion reactions on the solder's surface of the Sn-Zn-Cu alloys, with the focus on the role of copper in corrosion performance.

6.2 Results and Discussion

6.2.1 Metallographic analysis of Sn-9Zn-xCu solder alloys

The optical microstructure of Sn-9Zn-xCu ternary lead-free solder alloys is shown in Fig. 6.1. Sn-Zn alloys consist of three phases: black primary zinc, dark grey β-Sn, and light grey Sn-Zn eutectic phase. The shape, size, and distribution of both eutectics and β-Sn phase, which contained Zn-rich, β-Sn, and white Cu phase, were considerably altered by adding 1-3 wt. % Cu. The dark grey phase formed in the matrix after adding the third element Cu, as shown in Fig. 6.1 (b)-(d). With increasing Cu concentration, the quantity

of the dark grey phase increases, while the Zn phase's amount decreases, and then a more uniformly distributed eutectic structure appears. Therefore, a small amount of Cu can refine the microstructure. According to the Sn-Cu and Zn phase diagram, Cu might react with Sn and Zn to create form IMC; however, due to Zn's stronger reactivity, Cu will react with Zn rather than Sn [175]. Cu-Zn IMC is the newly identified phase corresponding to unique composition. Cu might react with Sn and Zn to form IMC. Fig. 6.3 shows the XRD pattern with copper variation in Sn-9Zn-xCu and binary Sn-9Zn alloy. In all the conditions, the primary phase was β-Sn with IMC, such as Cu_5Zn_8 and Cu_6Sn_5. In binary alloy, the primary phases were β-Sn and β-Zn. Cu added to the alloys appearance of copper-containing phases such as Cu_5Zn_8 and Cu_6Sn_5. Z.Wang et al.[74] Similar observations were also made. The XRD pattern corroborated this hypothesis. It can be deduced from the composition results that the intermetallic compound was Cu_5Zn_8.

For analyzing the formation of the eutectic phase, high magnification SEM images were taken, often etching of non-corroded samples. Fig. 6.2 shows a high magnification SEM image with varying copper content. The presence of Sn-Zn eutectic with a lamellar appearance in all situations can be observed in Fig. 6.2 (a-d) insight. The dark region is Sn, and the light region is Zn [176].

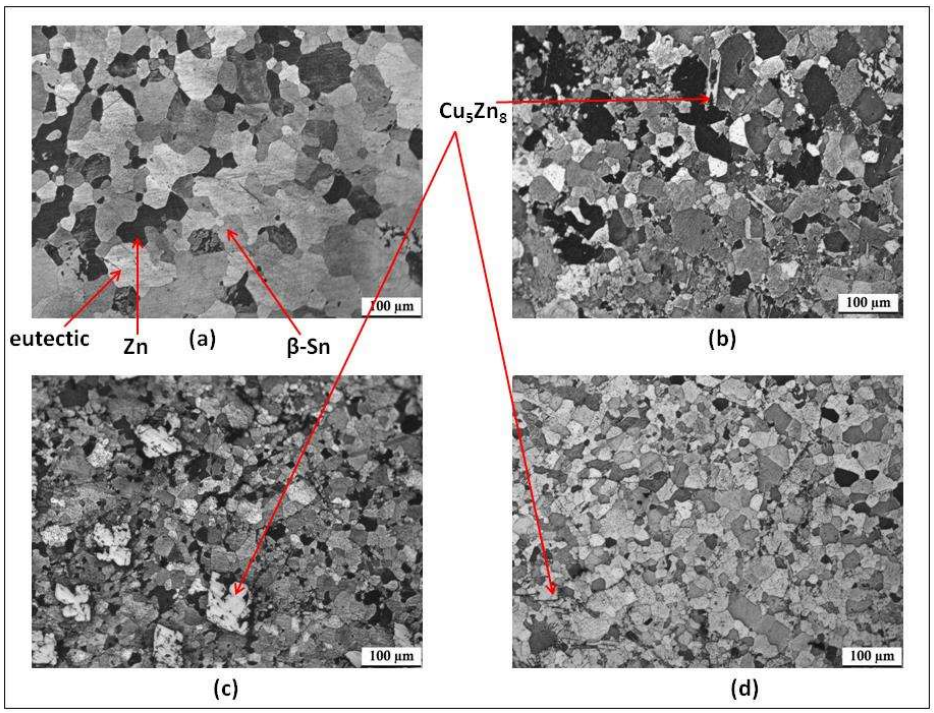

Fig.6. 1 Optical Microstructure of non-corroded Sn-9Zn-xCu alloys: (a) x=0, (b) x=1, (b) x=2 and (d) x=3.

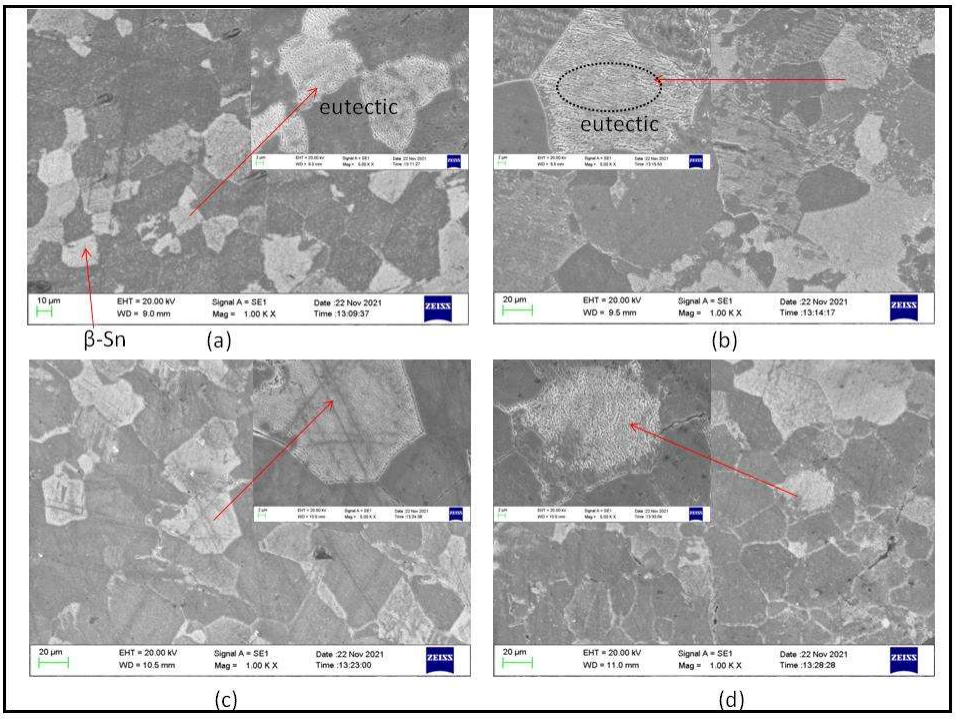

Fig.6. 2 SEM Microstructure of non-corroded Sn-9Zn-xCu alloys: (a) x=0, (b) x=1, (c) x=2 & (d) x=3.

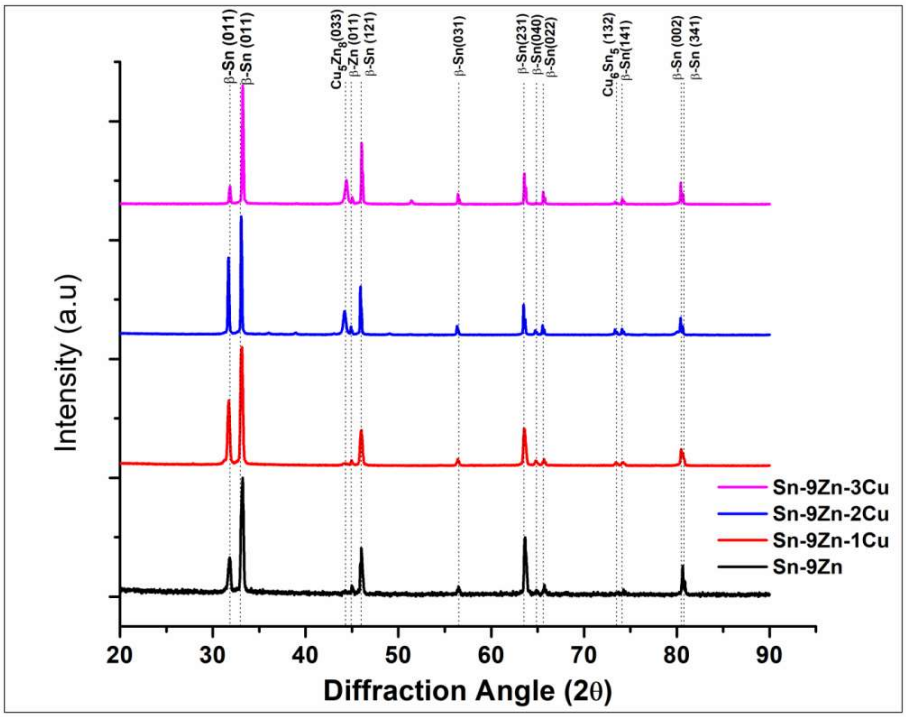

Fig.6. 3 XRD patterns of non-corroded Sn-9Zn-xCu alloys.

6.2.2 Immersion test

The rate of corrosion of Sn-9Zn-xCu alloys was assessed non-electrochemically using the traditional weight loss/gain approach. This method is used to calculate the loss of a metal due to corrosion by exposing a metal specimen of a specified area to a corrosive environment for a given time interval and calculating the weight difference before and after exposure. The most often used method of describing corrosion rate is millimeters per year (mm/yr). The formula is used to calculate the rate of corrosion.

$$CPR = \frac{KW}{\rho At}$$

Where K = constant and a value of 87.6 is taken as a present case.

W = Weight loss in grams

ρ = density of specimen in grams per cubic centimeter

A = expose area in a square centimeter

t = exposure time in an hour

The weight loss experiment of Sn-9Zn-xCu samples immersed in 3.5wt. % NaCl lasted 24 weeks; the results are presented in Fig. 6.4.

Up to 20 weeks, all of the samples demonstrated ongoing weight decrease. The binary Sn-9Zn solder alloy has seen the most weight reduction, whereas the ternary Sn-9Zn-xCu alloys experienced the least. A slight weight change can be seen in all of the samples after 8 weeks, which might be attributable to the formation of the oxide layer.

Fig. 6.5 shows cumulative weight loss after 24 weeks of exposure. It shows that 3wt.% Cu solder alloys show the least $(6.24 \pm 0.00167) \times 10^{-4}$ mm/yr, and binary Sn-9Zn alloys show the highest corrosion rate $(8.22 \pm 0.0059) \times 10^{-4}$ mm/yr.

Table 6. 1 Weight change of Sn-9Zn-xCu alloys after immersion in 0.5M NaCl solution

Times (Weeks)	**Weight Loss (mg)**			
	Cu(x=0)	**Cu(x=1)**	**Cu(x=2)**	**Cu(x=3)**
8	0.195	0.181	0.176	0.154
12	0.236	0.217	0.206	0.199
16	0.295	0.241	0.232	0.213
20	0.321	0.272	0.246	0.242
24	0.335	0.284	0.266	0.246

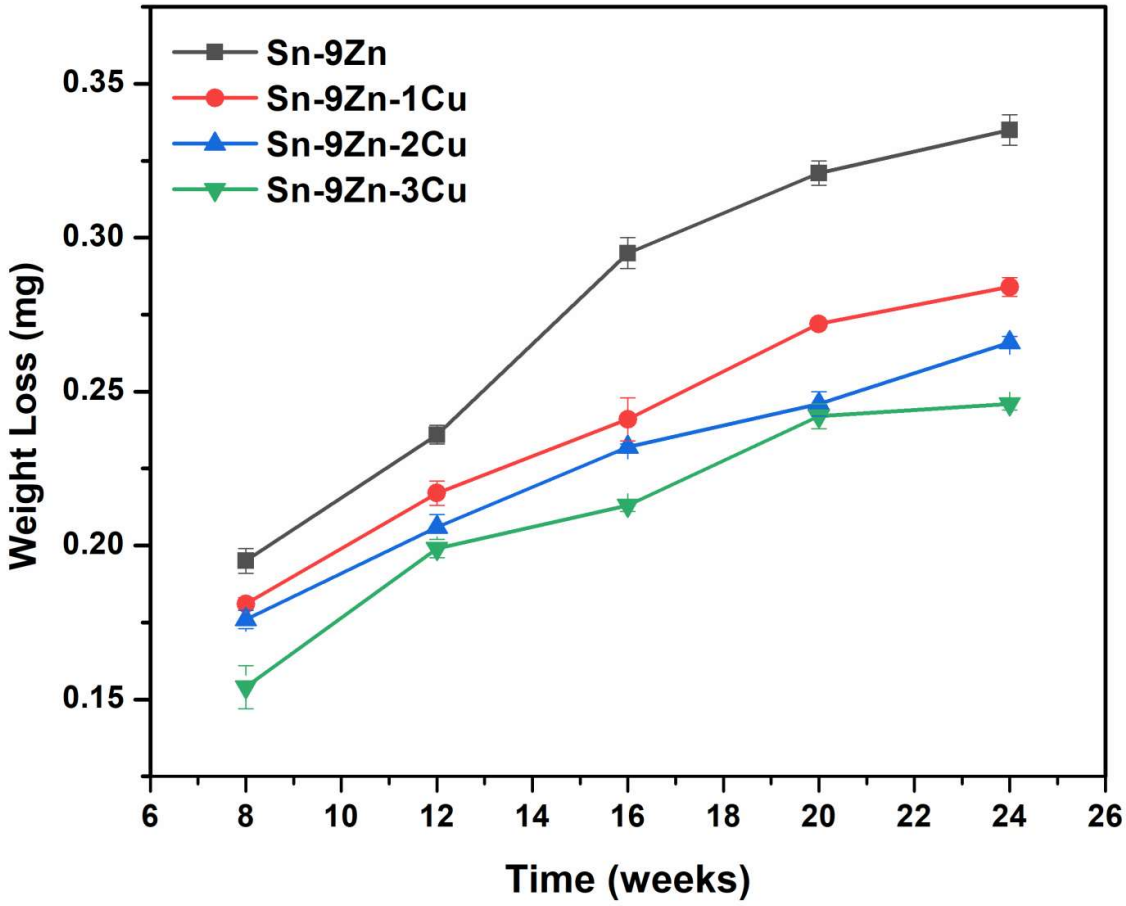

Fig.6. 4 Weight change of Sn-9Zn-xCu alloys after immersion in 0.5M NaCl at ambient temperature

Table 6. 2 Corrosion Rate of Sn-9Zn-xCu after immersion in 0.5M NaCl solution

S. No.	Samples	Corrosion Rates * 10^{-4} (mm/yr)
1	Sn-9Zn	8.266 ± 0.024
2	Sn-9Zn-1Cu	7.124 ± 0.021
3	Sn-9Zn-2Cu	6.680 ± 0.016
4	Sn-9Zn-3Cu	6.245 ± 0.019

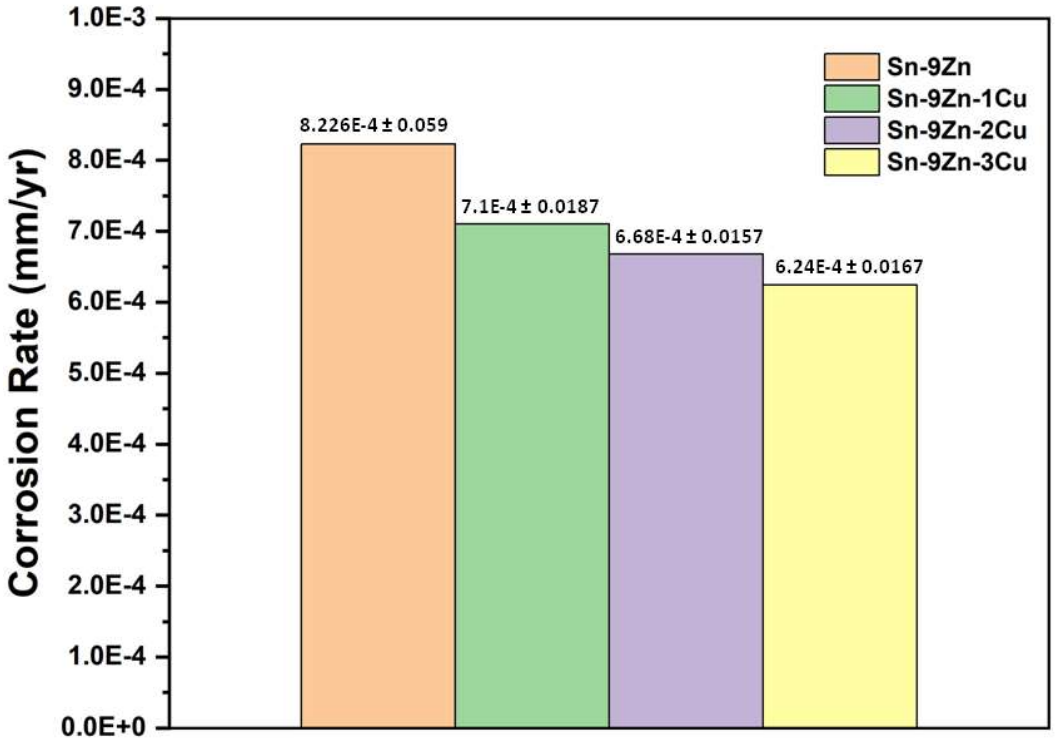

Fig.6. 5 Corrosion rate of Sn-9Zn-xCu alloys static immersion in 0.5M NaCl at ambient temperature

6.2.3 Open circuit potential and Potentiodynamic polarisation test

Fig. 6.6 illustrates the OCP versus function of time curves of the solder alloys recorded in 0.5M simulated NaCl solution at ambient temperature. In the all OCP test, it can be shown that the Sn-9Zn-3Cu has the more noble OCP values, followed by Sn-9Zn, Sn-9Zn-1Cu, and Sn-9Zn-2Cu. OCP test was measured for 3600 seconds, and the OCP of all solder alloys shifted in the region with more negative values of potential. Still, the OCP of copper-bested solder alloys is relatively tending nobler than the rest. Overall, Sn-9Zn-3Cu alloy showed the noblest value of OCP. This also indicates that the corrosion resistance of all alloys rises in the sequence of Sn–9Zn < Sn–9Zn-1Cu < Sn–9Zn-2Cu < Sn–9Zn-3Cu alloys, with the Sn–9Zn-3Cu alloy having the most substantial corrosion resistance.

Fig. 6.7 shown, the potentiodynamic polarization curves of Sn-9Zn-xCu alloys (x = 0.0, 1.0, 2.0, & 3.0 wt. %) in 3.5wt. % simulated NaCl solution. All Sn-9Zn-xCu alloys showed identical corrosion behaviour, as shown by identical polarisation curves. The cathodic branch A to B Point of polarization may be attributed to the reaction with oxygen (laboratory atmosphere) because the polarization studies were carried out in a static and naturally aerated sodium chloride solution at ambient temperature [177][178].

$$2H_2O + O_2 + 4e^- \rightarrow 4OH^- \quad (1)$$

All alloys showed dramatic increases in anodic current density when scanned in the anodic direction to the B to C point, owing to the active dissolution of the Zn and Sn phases according to reaction.

$$Sn \rightarrow Sn^{2+} + 2e^- \quad (2)$$

$$Zn \rightarrow Zn^{2+} + 2e^- \quad (3)$$

Zinc hydroxide is predicted to form when the hydroxide anion and zinc cation react. Near the interface, OH^- could react with Zn to form porous $Zn(OH)_2$, which would cover the interface, and the active dissolution of zinc in all of the experimental alloys continued to increase the potential for tested solder alloy samples until the zincate concentration reached a critical amount such as point C.

$$Zn^{2+} + 2OH^- \rightarrow Zn(OH)_2 \quad (4)$$

According to reaction 3, at particularly active cathodic sites, the pH may be high enough for zincate ions to form $Zn(OH)_2$. The insoluble zincate ions then coated the surface of the corroded samples and produced a plateau region in the CD range. At this point, it was discovered that the current density was independent of voltage throughout a 300mV range. Sn and/or Zn hydroxides or oxide production could be too responsible. The film's creation started with $Zn(OH)_2$ on the surface, which may later corrode ZnO. Because the

current density was high, the zinc oxidation film created in the C to D region was not passivation, according to Abayarthna et al. [19]. It may have protected the solder from further corrosion.

$$Zn(OH)_2 + 2OH^- \rightarrow Zn(OH)_4^{2-} \quad (5)$$

According to the reactions shown below, there is a rapid rise in current at -0.62V/(Ag/AgCl), which could be due to active Sn dissolution:

$$Sn + 2HO^- \rightarrow Sn(OH)_2 + 2e^- \quad (6)$$

$$Sn(OH)_2 \rightarrow SnO + H_2O \quad (7)$$

Following point D, the current density increased dramatically, indicating that the non-protective coating had broken down. This could be owing to the presence of Cl^- in the atmosphere/electrolyte, which is absorbed by corrosion products.

$$3SnO + 2Cl^- + 2H_2O \rightarrow Sn_3O(OH)_2Cl_2 + 2OH^- \quad (8)$$

$$5Zn(OH)_2 + 2Cl^- + H_2O \rightarrow Zn_5(OH)_8Cl_2.H_2O + 2OH^- \quad (9)$$

Boshkov et al. claim that Eq. (9), resulting in zinc hydroxide chloride in pits and nearby places, causes a local increase in pH value in the depth of corrosion damages.

Table 6.3 summarizes the detailed electrochemical parameters. The corrosion current density (i_{corr}) was calculated by extrapolating the cathodic Tafel line back to the corrosion potential E_{corr}. It was discovered that the Sn-9Zn-1Cu alloy had a lower i_{corr} value than the Sn-9Zn alloy, showing a propensity to reduce corrosion resistance after a minor quantity (1 wt%) of Cu addition. On the other hand, the corrosion resistance of the Cu-containing Sn-9Zn-xCu alloys increased as the Cu content was raised, and copper content increased from 1 to 3 wt.% The i_{corr} of the Sn-9Zn-3Cu alloy fell steadily from 10.731 μAcm^{2-} to 5.9075 μAcm^{2-}, with Cu having the lowest i_{corr}, suggesting the highest corrosion

resistance among these alloys. Corrosion rate value for Sn-9Zn, Sn-9Zn-1Cu, Sn-9Zn-2Cu and Sn-9Zn-3Cu are 0.15056, 0.12589, 0.11712 and 0.069303 mm/y respectively. As a consequence of the potentiodynamic polarization data, it is possible to deduce that corrosion resistance increased in the order Sn-9Zn < Sn-9Zn-1Cu < Sn-9Zn-2Cu < Sn-9Zn-3Cu.

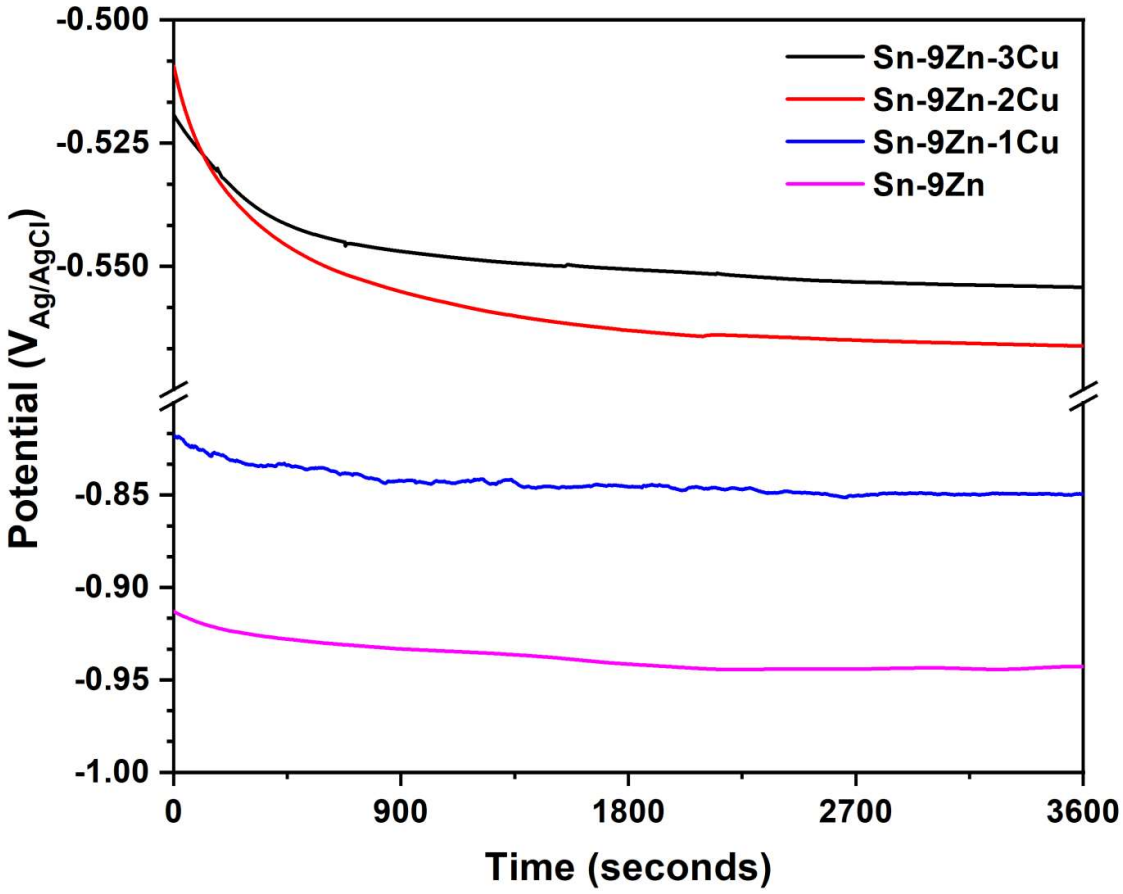

Fig.6. 6 OCP of Sn-9Zn-xCu alloys at 3600 seconds.

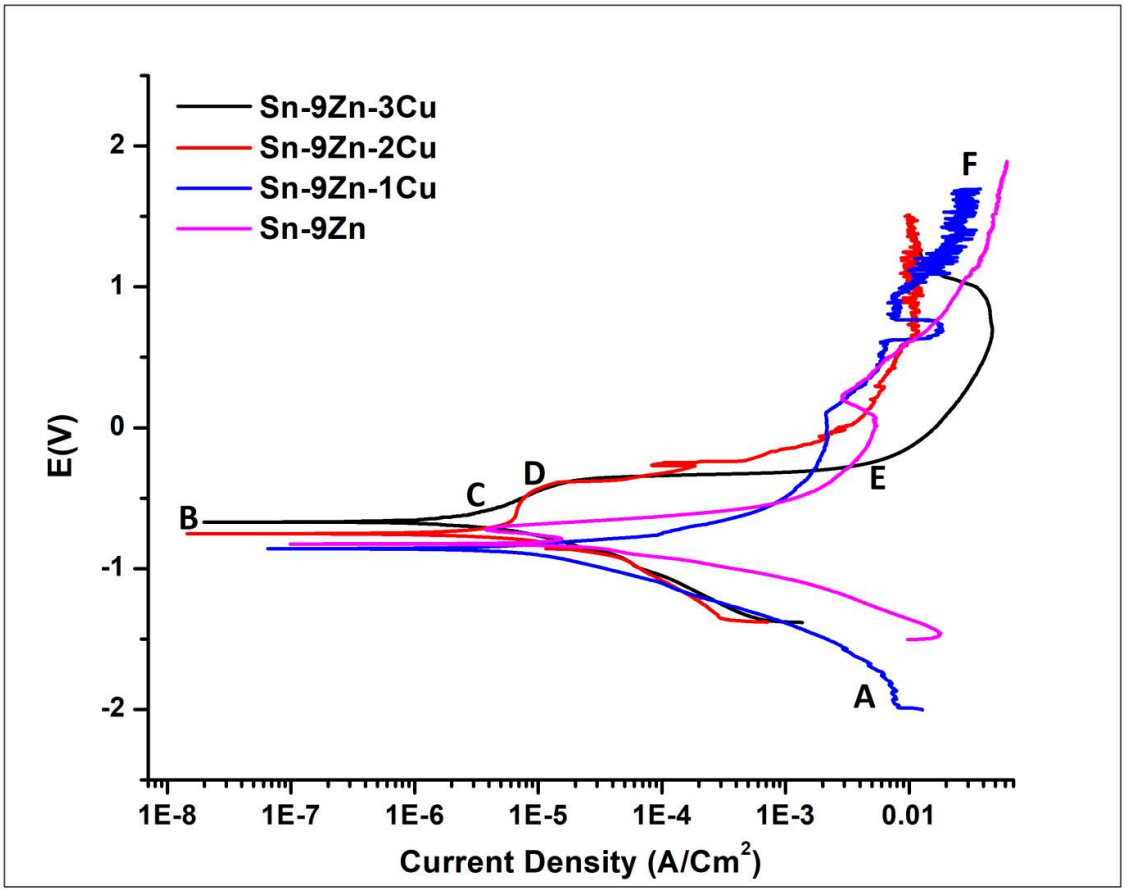

Fig.6. 7 Potentiodynamic polarization curves of Sn-9Zn-xCu alloys in 3.5 wt.% simulated NaCl.

Table 6. 3 Polarization parameters for Sn-9Zn-xCu alloys in 3.5 wt.% simulated NaCl.

Samples	β_a(mV)	β_b(mV)	I_{corr}(Amps/Cm^2)* 10^{-6}	E_{corr}(Volts)	Corrosion Rate (mm/y) x 10^{-2}
Sn-9Zn	4736.6	264.15	12.834	-0.75238	0.15056
Sn-9Zn-1Cu	56631	344.04	10.731	-0.66993	0.12589
Sn-9Zn-2Cu	124.62	257.92	9.9835	-1.0586	0.11712
Sn-9Zn-3Cu	512.73	101.55	5.9075	-1.2246	0.069303

6.2.4 Electrochemical impedance spectroscopy Analysis

In a 3.5 wt.% simulated NaCl solution, the Nyquist and Bode plots of Sn-9Zn-xCu (x = 0, 1.0, 2.0 & 3.0 wt. %) alloys at their open circuit potential are shown in Fig. 6.8 and Fig. 6.9 respectively. As illustrated in Fig. 6.8, each Nyquist plot was found to be made up of

capacitive semi-arcs. The arc radius of the Sn-9Zn alloy was the smallest, indicating that it had the lowest corrosion resistance of the alloys studied. With increased Cu 1 to 3 wt. percent in binary Sn-9Zn solder alloy. The copper-containing Sn-9Zn-xCu alloy had a wider capacitive arc radius.

Furthermore, the Bode plots of |Z| vs. frequency shown in Fig. 6.9(a) and the highest Cu contents alloys showed higher impedance values in the Cu-containing alloys, implying that Cu adding (1 to 3 wt.%) might reduce the corrosion vulnerability of the Cu containing Sn-9Zn-xCu solder alloys. At low frequencies, Bode curves (fig. 6.9(a)) reveal that Sn-9Zn-3Cu has the highest |Z| value, corresponding to the greatest capacitive semi-circle. These events were found to be consistent with the outcome of polarization analysis. Focusing on the phase angle plots in Fig. 6.9(b), two peaks can be seen between 100 kHz and 0.1 Hz, indicating the presence of 2-time constants, which correspond to two capacitive loops in Fig. 6.9(a). The electrical double layer generated at the interface between the corrosion product and alloys is responsible for the time constant at low frequencies.

The development of corrosion products is linked to the capacitive semi-circle at a high frequency[179]. Fig. 6.10 depicts two alternative equivalent electrical circuits (EEC) that were employed to suit the experimental points in this investigation. Table 6.3 summarizes the fitted EIS findings. The fit quality was assessed using chi-squared (χ^2) values, which were all in the range of 10^{-4} to 10^{-3} in all cases. R_s represent the uncompensated solution resistance in the EEC. As demonstrated in Fig. 6.10, existing systems do not behave like an ideal capacitor; thus, in the equivalent circuit, a constant phase element (CPE) was utilized instead of a pure capacitor to better suit the impedance behaviour. The constant phase element (CPE) is linked to scattered, inhomogeneity, electrode porosity, surface reactivity, roughness, and species adsorption [160]. The corrosion product layer's

resistance and capacitance are represented by R_1 and CPE_1. The capacitance and resistance of the electrical double layer between the interface of corrosion products and alloy are represented by CPE_2 and R_2. W stands for the Warburg impedance, which describes charge species diffusion at the contact.

The findings in Fig. 6.10 and Table 6.4 revealed that Sn-9Zn had a substantially lower charge transfer resistance (R_2). Corrosion resistance is increased when the capacitance arc radius is bigger. However, in Cu-containing alloys, considerable increases in R_2 were found when the copper content was raised from 1 to 3 wt.%, showing that the charge transfer mechanism was made more complex by adding additional Cu. The existence of diffusion-controlled impedance was seen when 3 wt% Cu was added, suggesting that the corrosion mechanism of the new alloy was regulated by both diffusion processes and charge transfer [75][72]. The presence of Warburg resistance (R_w) revealed that the transfer of charge species in the Sn-9Zn-3Cu alloy was significantly highest [73]. Total resistance (R_t) can be derived from R_1, R_2, and R_w (diffusion resistance) to measure overall corrosion resistance, according to the EEC (ignore the solution resistance). Sn-9Zn alloys had a low $R_t = R_1+R_2+ R_w$[162] value of 2519.4 Ω-cm^2, indicating a lower corrosion resistance. At the same time, the overall impedance increased when a small quantity of Cu was introduced into the Sn-9Zn binary solder alloy. The R_t values for Sn-9Zn-1Cu, Sn-9Zn-2Cu, and Sn-9Zn-3Cu were relatively higher, 5.4592, 14.080, and 30.266 KΩcm^2, respectively, showing that a larger amount of Cu added increased corrosion resistance. It was evident that Sn-9Zn-3Cu had the best corrosion resistance among all these alloys. Therefore, the corrosion resistance improved in the sequence of Sn-9Zn, Sn-9Zn-1Cu, Sn-9Zn-2Cu, and Sn-9Zn-3Cu, as indicated by the EIS data. This was in line with polarization measurements, which confirmed the findings.

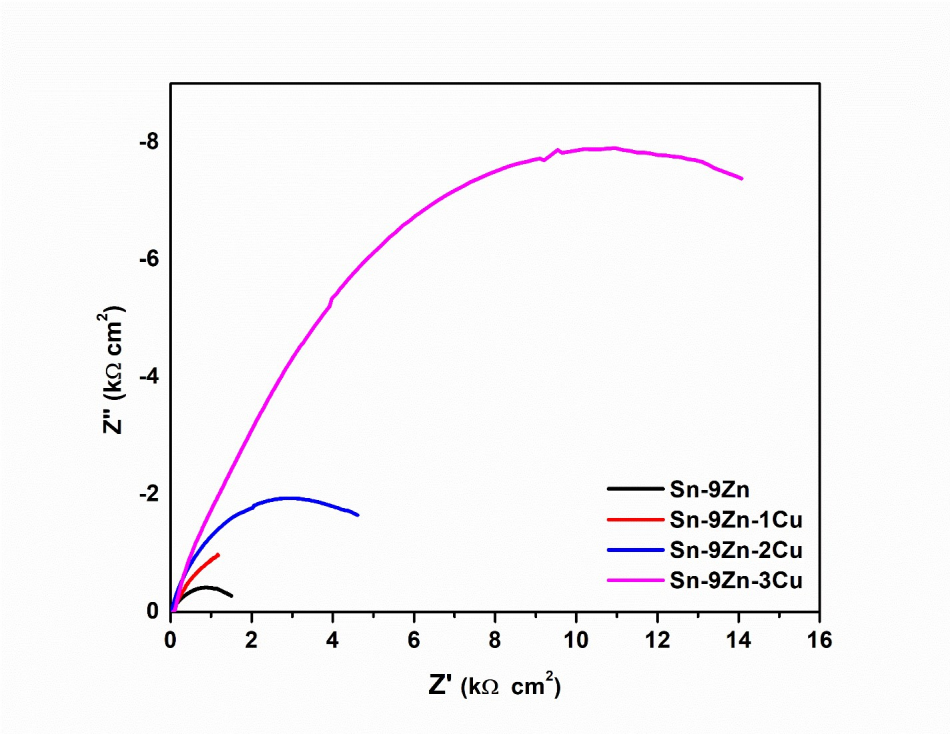

Fig.6. 8 Nyquist of Sn-9Zn-xCu solder alloys in 3.5 wt.% simulated NaCl.

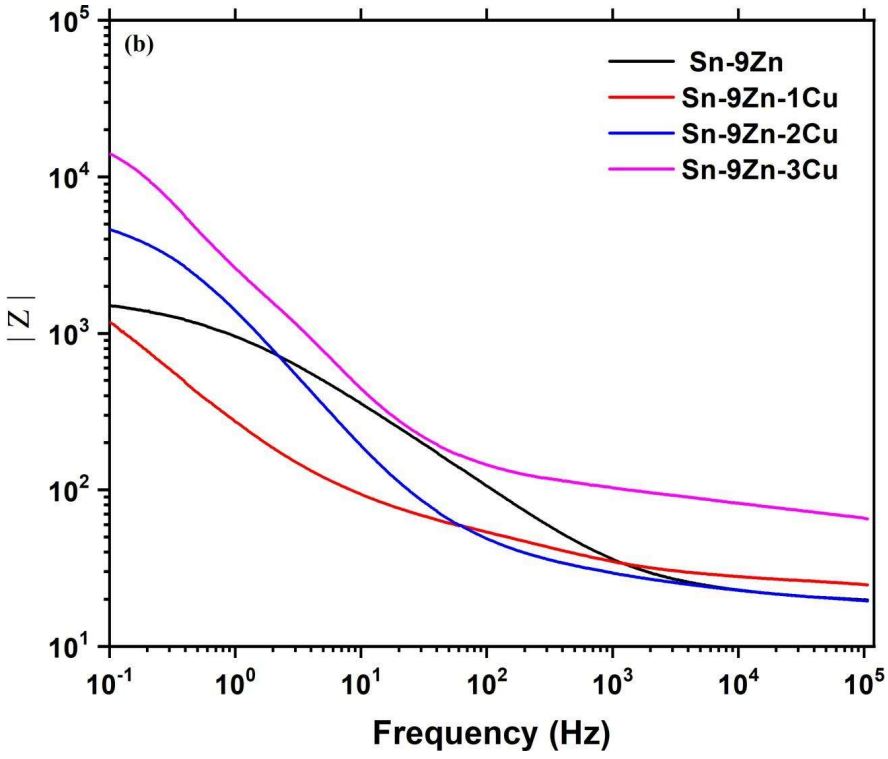

(a)

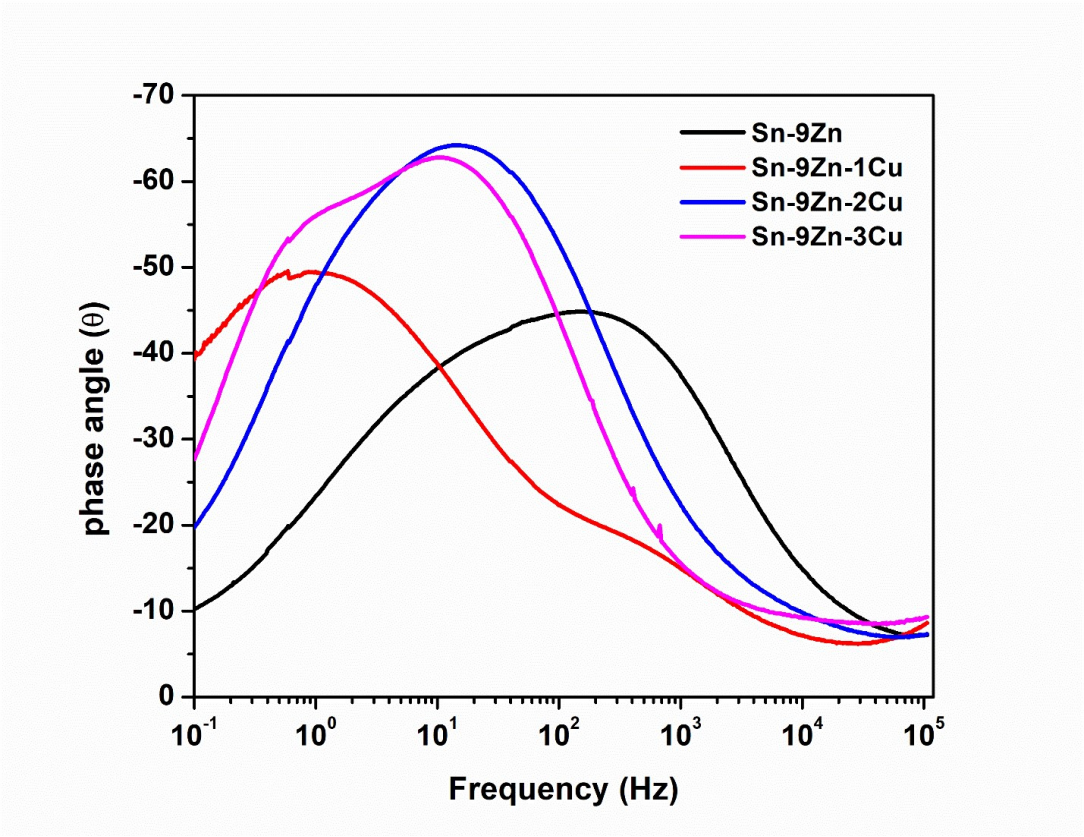

(b)

Fig.6. 9 Bode plots (b,c) of Sn-9Zn-xCu solder alloys in 3.5 wt.% simulated NaCl.

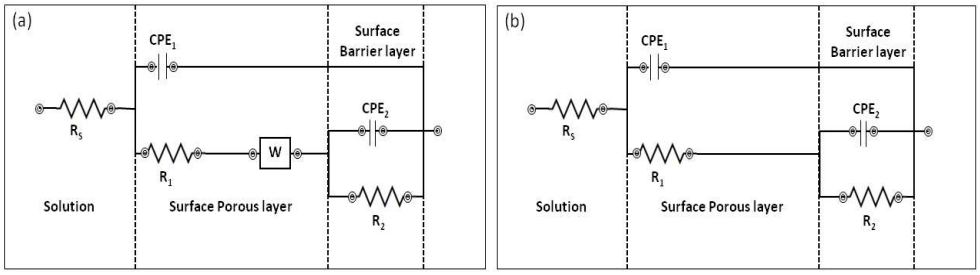

Fig.6. 10 Electrical circuit models of Sn-9Zn-xCu (a)x=0,(b) x=1,2&3 wt.%

Table 6. 4 Fitting parameters of EEC for Sn-9Zn-xCu solder alloys in 3.5 wt.% simulated NaCl

Sample	R_s Ωcm^2	R_1 Ωcm^2	CPE_1		R_2 Ωcm^2	CPE_2		R_w Ωcm^2	$\chi^2 * 10^{-4}$
			Y_1*10^{-6} $\Omega cm^{-2}s^n$	n_1		Y_2*10^{-6} $\Omega cm^{-2}s^n$	n_2		
Sn-9Zn	17.52	699.4	102.0	0.64	1820	210.5	0.67		14.409
Sn-9Zn-1Cu	18.31	918.2	868.19	0.60	3376	995.581	0.93	1165	10.49
Sn-9Zn-2Cu	16.87	4527	84.28	0.80	6074	100.67	0.73	3479	21.23
Sn-9Zn-3Cu	16.41	8125	40.537	0.79	13368	46.925	0.81	8773	15.18

6.2.5 Characterization of Corrosion product

Fig. 6.10 depicts a typical corroded surface of solder alloy Sn-9Zn-xCu (x=0, 1, 2 & 3 wt.%); after polarization measurement, morphological and chemical composition analysis were done by EDX and SEM, respectively. The surface of the alloys changed rapidly from smooth to porous as it was exposed to the 0.5M NaCl solution, with the production of platelet and sponge, crystallites, and networked branched structures forming as a result of the weakly bound corrosion products on the surface. These chemical compounds have been recognized as oxides, and hydroxides by EDS and XRD are typical corrosion products.

The badly corroded region shown by the black contrast (Fig. 6.11) was mostly made up of Zn, Cl, and O components, suggesting that corrosion products were primarily made up of these elements. The brightness contrast in Fig. 6.11 represents a corroded region with many Sn and a tiny quantity of O. As a result, it was inferred that the Zn phase, rather than Sn, was selectively preferentially corroded by Cl^- and OH^- anions.

After polarisation tests, the XRD patterns of the corroded surface of Sn-9Zn-xCu (x = 0, 1, 2 & 3 wt.%) solder alloys are shown in Fig. 6.12 to validate the phase composition of

corrosion products. After polarisation studies, it was discovered that the β-Sn phase persisted in all cases; however, the Zn phase was barely detectable, indicating that the Zn-rich phase was substantially consumed. Cu phase was found in abundance in Cu-containing alloys with Cu concentrations of more than 1 wt%, showing the difficulties of corroding Cu in 3.5 wt.% simulate NaCl solution because of its comparably stronger corrosion potential than Zn and Sn. The primary corrosion product for all Sn-9Zn-xCu solder alloys has been recognized as complexed zinc hydroxyl chloride hydrates ($Zn_5(OH)_8Cl_2H_2O$). In addition, a tiny quantity of SnO, ZnO, CuO and $Sn_3O(OH)_2Cl_2$ was detected.

The corroded zone was covered in loosely aggregated plate-like formations that were identified as simonkolleite $Zn_5(OH)_8Cl_2H_2O$ by EDXS analysis[124]. This was supported by the XRD results. The initial Zn-rich needles were depleted and dissolved, leaving narrow channels on the surface, as indicated by EDXS analysis, indicating that Zn-rich phase destruction is more accessible than Sn phase destruction. In addition, a corrosion product with a sphere-shaped morphology was discovered in the aggregate of the ZnO plates.

It has been established that a small quantity (1-3 wt percent) of Cu addition to the Sn-9Zn alloy can induce increased corrosion resistance based on polarization and EIS data. Also, when copper weight percentage increases, corrosion products on solder alloys become denser, continuous and refined. The corrosion resistance of Sn-9Zn-3Cu alloy was more excellent than other alloys of Sn-9Zn-xCu. In the Sn-Zn solder alloys system, zinc is more active than Sn because Zn has a higher negative electrode potential (-0.763 V versus SHE) than Sn (-0.136 V versus SHE); Zn-rich precipitates behave as active anodes in the Sn-Zn system and can be corroded preferentially under corrosive conditions. The dissolution of Zn at anodic sites initiates the corrosion process.

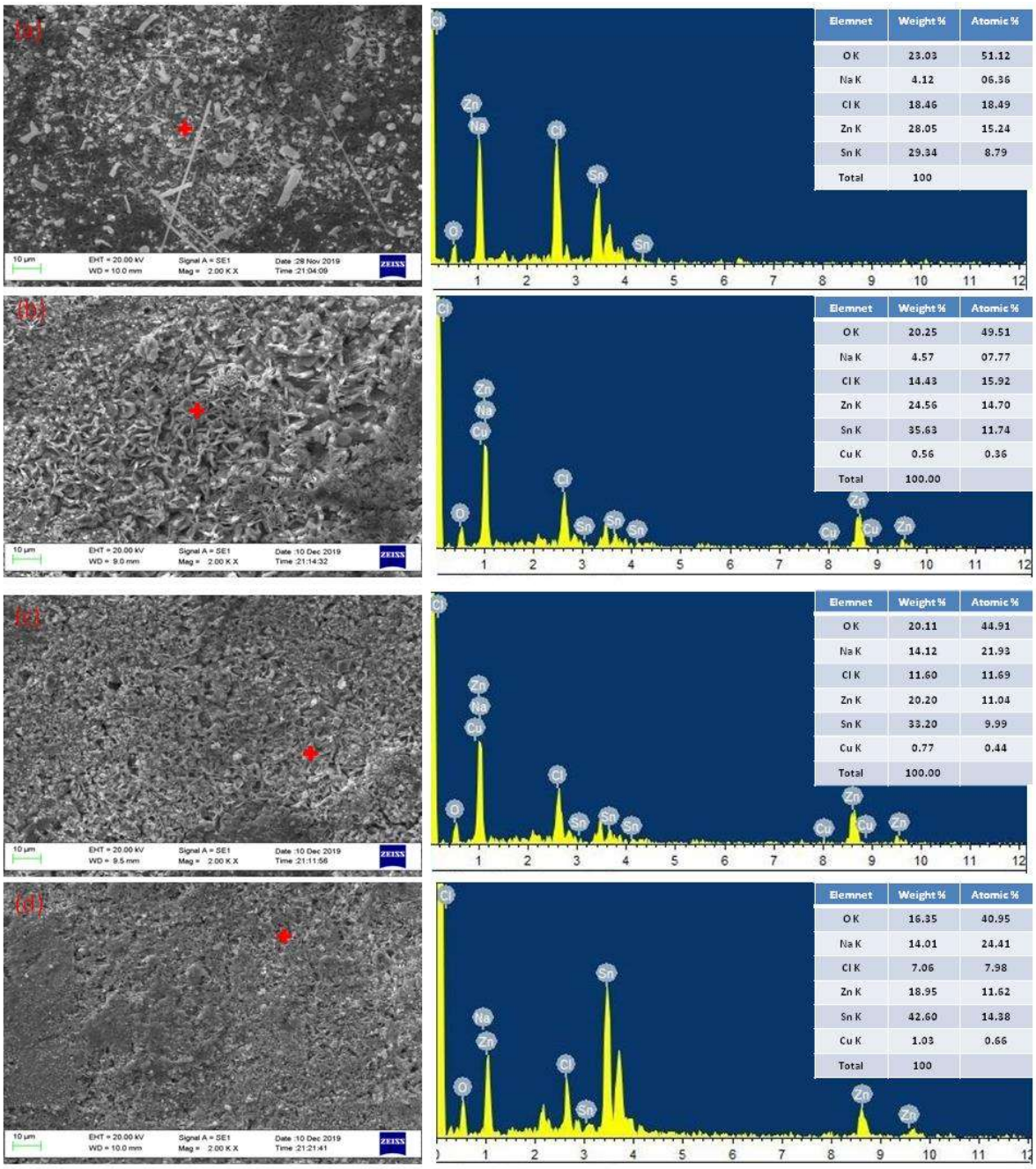

Fig.6. 11 SEM-EDX analysis of the corroded surface of Sn-9Zn-xCu solder alloys. (a) x=0, (b) x=1, (c) x=2 & (d) x=3.

The initial Zn-rich precipitates might be selectively degraded in this manner, leaving the Sn phase (cathode) intact. Further electrochemical reactions occur with the addition of water and oxygen, resulting in the formation of zinc oxide and/or zinc hydroxide.

In the presence of Cl, Cl^- will migrate towards Zn dissolving sites, especially if the chloride concentration is over 0.1M, resulting in the progressive production of insoluble zinc hydroxy chloride. The XRD and EDS composition analyses quickly identified these corrosion products as $Zn_5(OH)_8Cl_2.H_2O$, $Sn_3O(OH)_2Cl_2$, SnO, and ZnO. In this case, it's expected that $Zn_5(OH)_8Cl_2.H_2O$ will form around the anodic sites.

When copper was added to Sn-9Zn-xCu(x=0.0, 1.0, 2.0 & 3.0 wt.%) solder alloys, the size of Zn-rich precipitates grew significantly, and their distribution became more uniform. Because of the poor link between the coarse β-Sn matrix and Zn-rich precipitates, those of bigger size may degrade corrosion performance. Because of the poor link between the coarse Zn-rich precipitates and the β-Sn matrix, those of more significant size may degrade corrosion performance. This was predicated on the assumption that defects (such as voids and dislocations) might easily collect along with the interface between the coarse β-Sn phase and Zn-rich precipitate. As a result, the flaws accumulated sites may aid in the movement of OH^- or Cl^- inwards and stimulate chemical reactions between the Zn-rich phase and anions, enhancing corrosion rates. On the other hand, pitting at the sensitive Zn/Sn contact might be very susceptible to start and spread. Liu et al. [75] discovered a similar effect, demonstrating that adding a minor amount of Ag, Cu, Cr, and Ni to the Sn-9Zn solder alloy improves corrosion resistance due to the removal of massive Zn precipitates.

In the Sn-9Zn-3Cu alloy, a substantial fraction of β-Sn functioning as noble cathodes spatially and largely separated the high corrosion areas, i.e., Sn-Zn eutectic "islands". These imply that the noble β-Sn phase could operate as a corrosion barrier, preventing corrosion. In the Sn-9Zn alloys, on the other hand, the Zn-rich region was distributed much more uniformly, indicating that there were more corrosion-vulnerable locations present and fewer percentages of effective anodic barriers.

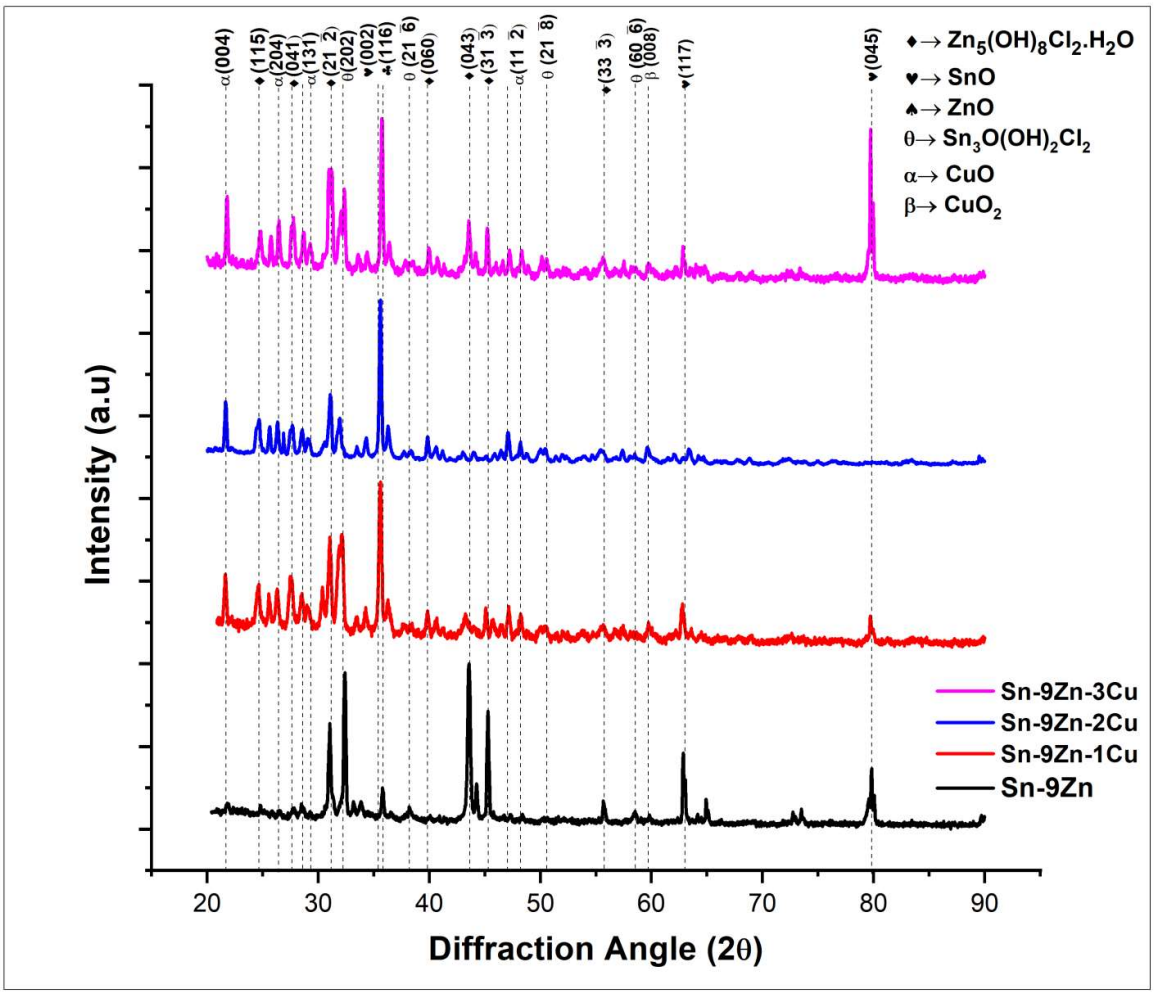

Fig.6. 12 XRD pattern of the corroded surface of Sn-9Zn-xCu solder alloys.

Zn $2p_{3/2}$ spectra of the corroded surface of Sn-9Zn-xCu solder alloy in 3.5 wt.% simulated NaCl solution were observed in XPS surface analysis and shown in Fig. 6.13.

With binding energy of 1021.3 ± 0.5 eV, ZnO peaks were observed at all the sample surfaces. With varying Cu in Sn-9Zn-xCu solder alloy, ZnO peak intensity also decreases, suggesting lower corrosion intensity for a higher Cu content sample [180]. Also, from the potentiodynamic polarization test, i_{corr} reduces with increasing Cu content, lowering corrosion rates. The Fig. 6.13 also shows that the Sn $3d_{5/2}$ spectra of the corroded surface of Sn-9Zn-xCu solder alloy are 3.5 wt.% NaCl electrolytic solution. In all the cases,

metallic Sn^0 with $Sn^{+2/+4}$ was observed at a binding energy of 485.02 ± 0.5 eV, and 486.9 ± 0.5 eV was observed at the surface [181]. It suggests that formation of tin oxide in the form of SnO and SnO_2 since both the tin oxide may overlap due to minor differences in binding energy. Metallic Sn was there in all the cases, which suggested that either the formed oxide layer was not uniform or due to action of Cl^- resulted in breakage of the oxide layer leading to the interaction metallic of Sn with photoelectron during XPS analysis. The increase of Cu in Sn-9Zn-xCu leads to a decrease in intensity of the formed oxide layer, which shows lower corrosion rates for higher Cu contents samples in line with the X-ray diffraction and potentiodynamic polarization data. The Fig. 6.13 also reveals that the Cu 2p3/2 spectra of Sn-9Zn-XCu solder alloys are 3.5 wt.% NaCl simulated solution. It clearly shows that the intensity of Cu peaks increases on increasing the Cu content. Metallic Cu was present in all the cases at a binding energy of 952.58 and 932.68 eV, respectively[60], indicating the formation of Cu^0. Its shows the Cu_5Zn_8 phase, which was also confirmed by X-ray analysis. With an increase in Cu content, it can be seen that the formation of Zn oxides gets diminishes, which shows that Cu addition makes oxidation of Sn difficult.

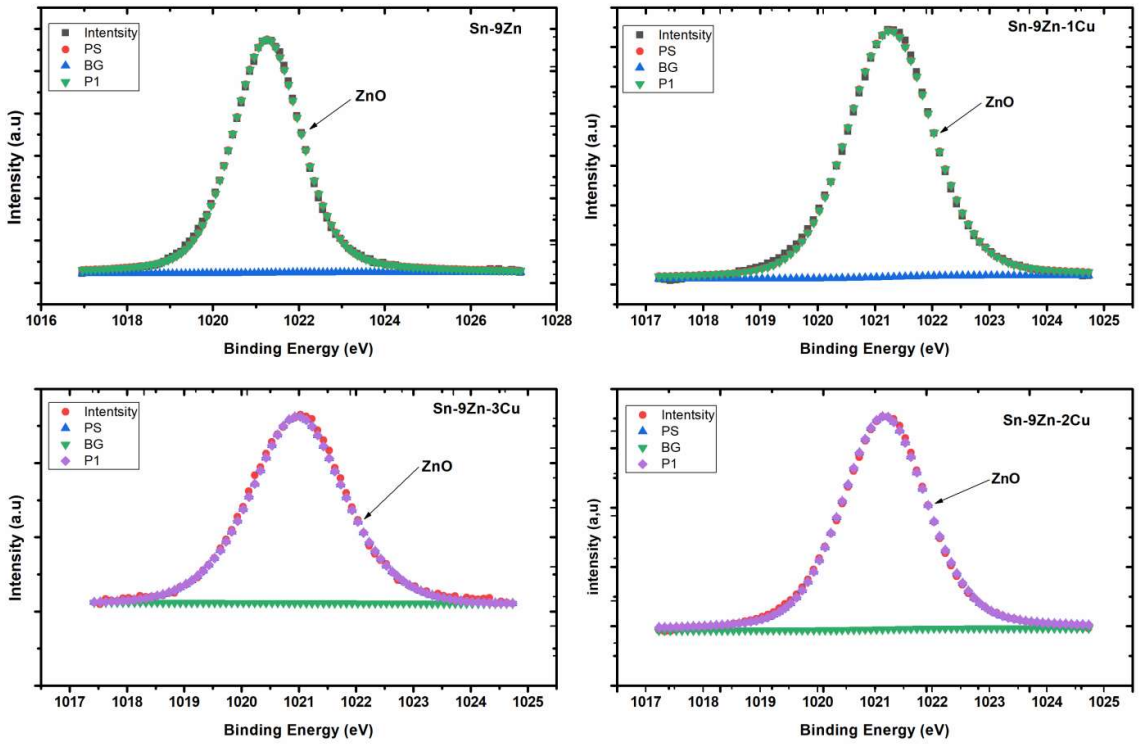
Intentsity
PS
BG
P1
Sn-9Zn
ZnO
Intensity (a.u)
Binding Energy (eV)
Sn-9Zn-1Cu
Sn-9Zn-3Cu
Sn-9Zn-2Cu
intensity (a.u)

(a)

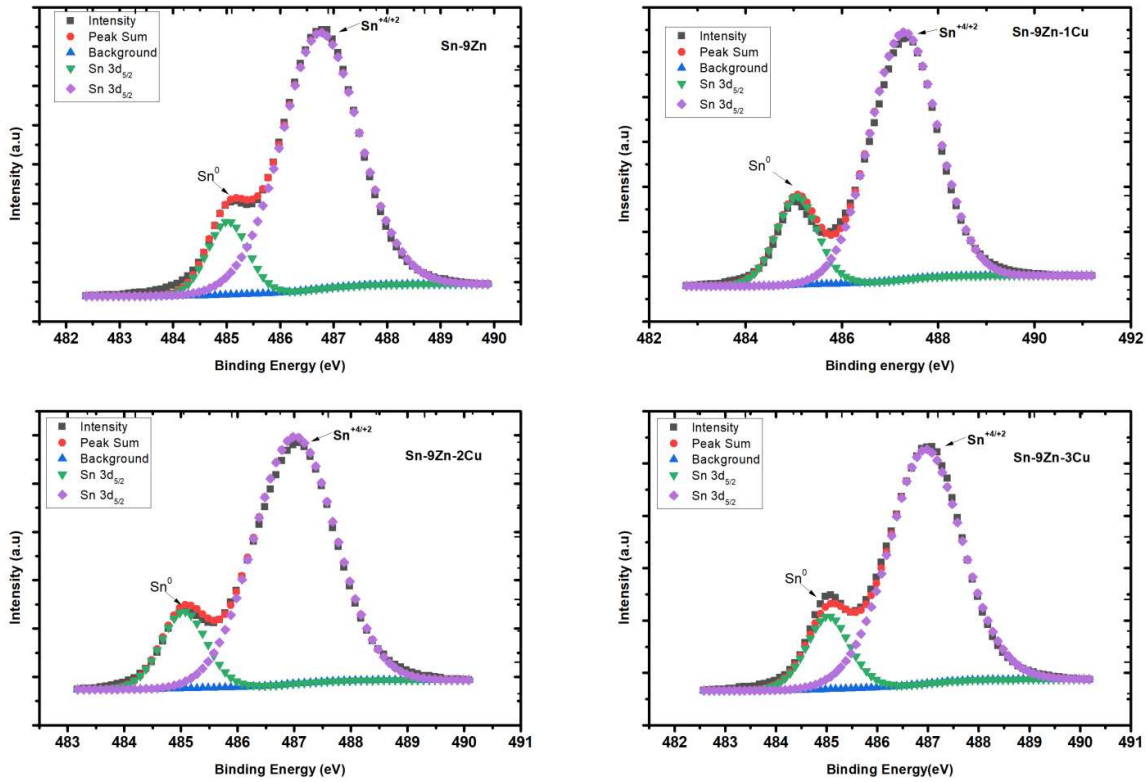
Intensity
Peak Sum
Background
Sn 3d5/2
Sn 3d5/2
Sn+4/+2
Sn0
Sn-9Zn
Intensity (a.u)
Binding Energy (eV)
Sn-9Zn-1Cu
Insensity (a.u)
Binding energy (eV)
Sn-9Zn-2Cu
Sn-9Zn-3Cu
Binding Energy(eV)

(b)

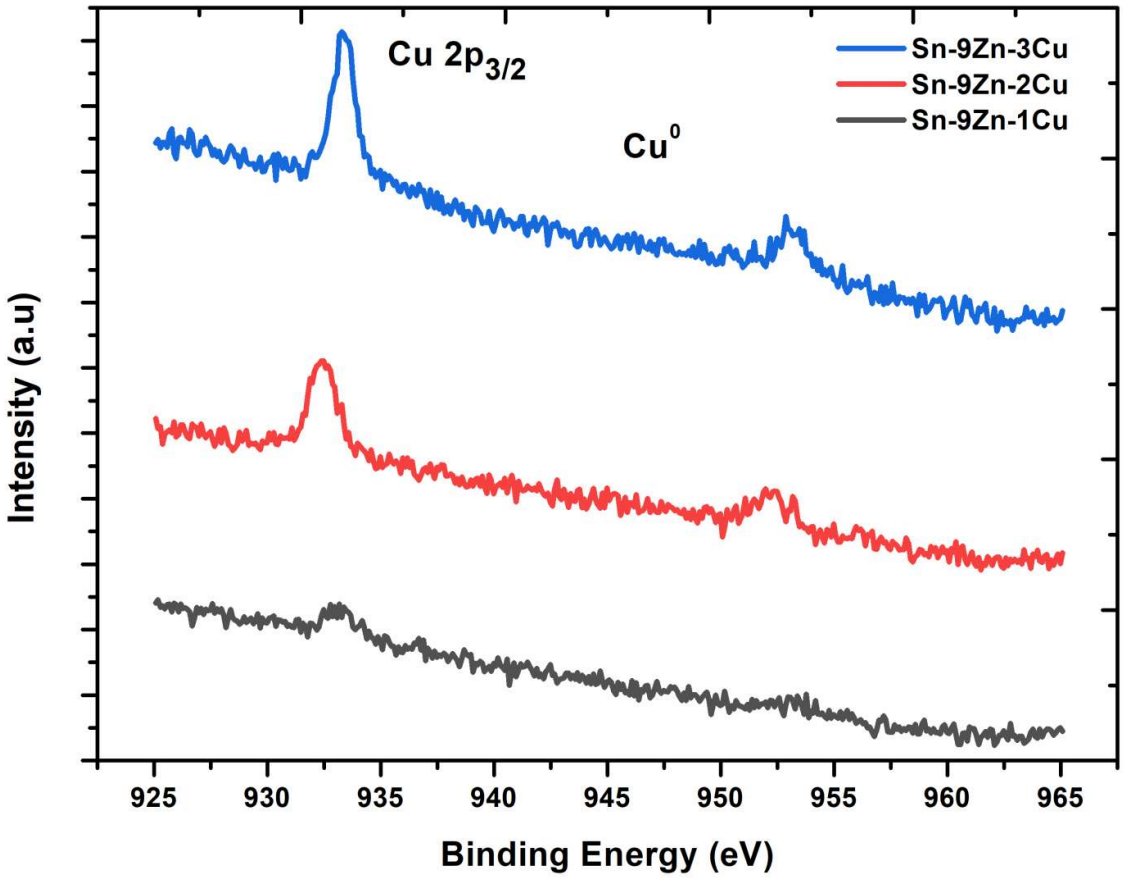

(c)

Fig.6. 13 The XPS profiles of Sn-9Zn-xCu alloys after corrosion tests.
(a)Zn2p (b)Sn 3d,(c) Cu 2p.

6.2.6 Corrosion mechanism

The corrosion of Sn-9Zn-xCu alloys occurs in 3.5 wt.% NaCl electrolyte solution, as shown in Fig. 6.14. The development of pitting corrosion can be divided into three phases (a) passive film breakage, (b) Initiation of pits (c) growth of pits. Hence from the potentiodynamic plots, we can see that all the solder alloys follow passivation. Passive film breakage can be occurred by the dissolution of passive film in the form of hydroxide ($Zn(OH)_2$, $Sn(OH)_2$); also, from the defect site, Cl^- ions increase into the passive layer, leading to breakage and increase of Sn^{2+}/Zn^{2+} concentration in the electrolyte. Once the passive layer breaks, the active dissolution of Zn-rich participants starts, leading to pit formation at the surface; this stage is known as the pit initiation stage.

Further thinning of the passive layer cause increased autocatalytic dissolution of metal ions in the vicinity of the pits, resulting in an increase in acidity in the vicinity of the pits; also, the increase in metal ion concentration near the pits accelerates the pitting process in a transitive direction. Accumulation of corrosion product at the edge wall of the pits formed. Stage causes the increase in the concentration of OH^- species in the vicinity of the pit. This will lead to an autocatalytic ion transfer reaction at a stable rate.

There is an increase in the diffusion of OH^- into the metal ion concentration region, and there will be a decrease in the pH of the solution. Also, at the same time, active dissolution in the vicinity will result in stable pit growth.

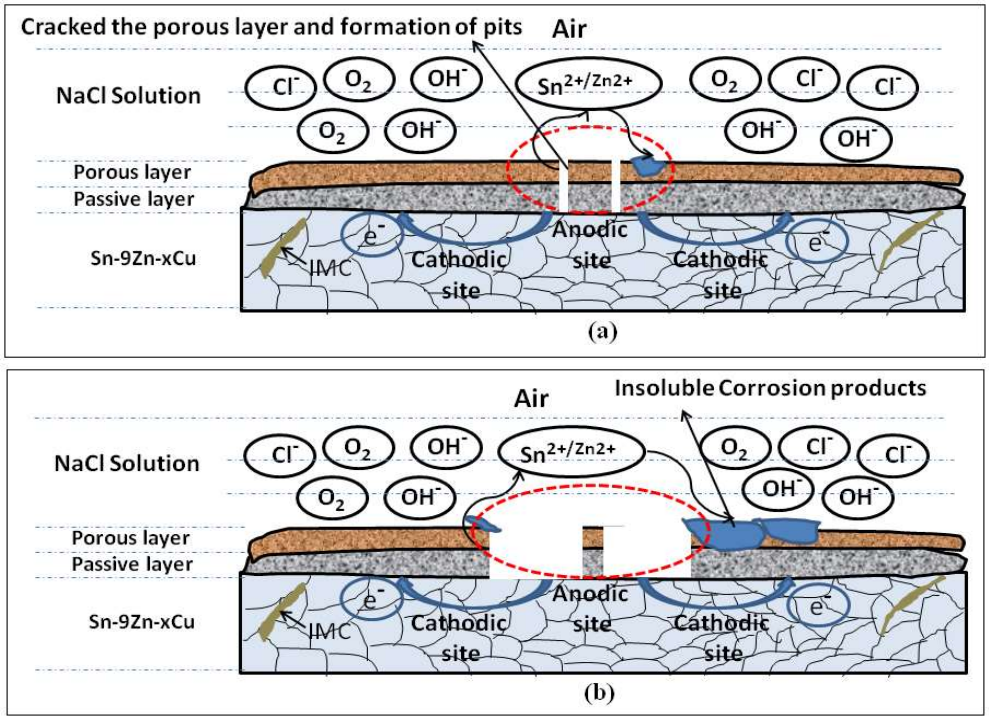

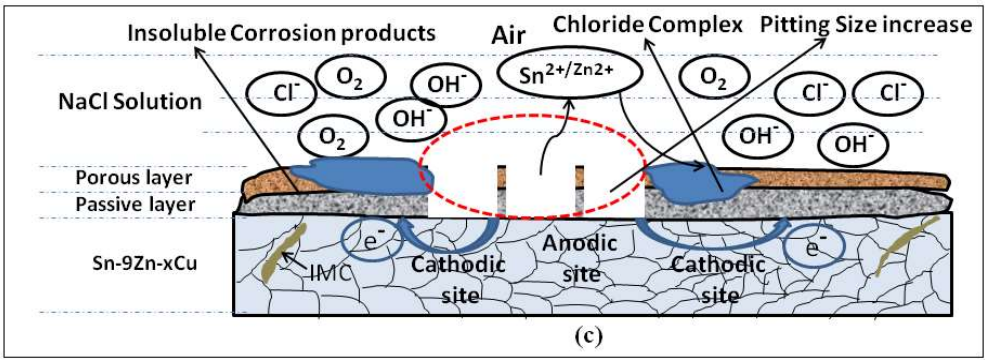

Fig.6. 14 Corrosion Mechanism of Sn-9Zn-xCu alloys (a) passive film breakage, (b) Initiation of pits, (c) growth of pits.

6.3 Conclusions

The electrochemical corrosion behaviour and corrosion mechanism of lead-free Sn-9Zn-xCu solder alloy were investigated in 3.5wt.% NaCl solution at ambient temperature using potentiodynamic polarization, immersion test, and EIS techniques with a combination of SEM, EDX, XPS, and XRD analyses, and the following significant conclusions were derived:

1. The Corrosion rate observed from the potentiodynamic polarization test reveals that the highest corrosion rate (0.15056×10^{-2} mm/y) was observed for the Sn-9Zn alloy and the lowest (0.0693×10^{-2} mm/y) for that of Sn-9Zn-3Cu. The immersion test and EIS measurements revealed a similar trend in the corrosion performance of the Sn-9Zn-xCu alloy in 0.5M NaCl solution.
2. The inclusion of copper in Sn-9Zn solder binary solder alloy resulted in a more uniform distribution of intermetallic phase and refined microstructure, which is responsible for improving corrosion resistance.
3. The corrosion of the alloys occurs due to the integration of Cl^- ions that results in passive film breakdown followed by the selective dissolution of IMC, resulting in pits formation and growth.

4. Corrosion product formation on the surface of alloys was primarily zinc hydroxide chloride ($Zn_5(OH)_8Cl_2.H_2O$), tin oxide chloride hydroxide ($Sn_3O(OH)_2Cl_2$), tin oxide (SnO), and zinc oxide (ZnO) have plate-like forms. They are strewn across the surface in a variety of positions.